Euphotic Zone Depth Anomaly in Global Mesoscale Eddies by Multi-mission Fusion Data

Yan Wang[1, 3], Jie Yang[1, 2*]

[1]School of Marine Technology, Ocean University of China, Qingdao, China.

[2]Laboratory for Regional Oceanography and Numerical Modeling, Qingdao National Laboratory for Marine Science and Technology, Qingdao, China.

[3]Academy of the Future Ocean, Ocean University of China, Qingdao, China.

Corresponding author: Jie Yang (yangjie2016@ouc.edu.cn)

Key Points:

- Anticyclones mainly deepen the euphotic zone depth, while cyclones do the opposite.
- Eddy-induced euphotic zone depth anomalies reach a maximum at around 40 degrees.
- Eddy-induced euphotic zone depth anomalies are inversely correlated with chlorophyll concentration.

Abstract

As the waters of marine primary production, the euphotic zone is the primary living environment for aquatic organisms. Eddies account for 90% of the ocean's kinetic energy and affect marine organisms' habitats by the excitation of vertical velocities and the horizontal advection of nutrients and ecosystems. Satellite observations indicate that anticyclones mainly deepen the euphotic zone depth, while cyclones do the opposite. Eddy-induced euphotic zone depth is inversely correlated with the eddy-induced chlorophyll concentration. The anomalies reach 5m on average in the region of high eddy amplitude and frequent eddy occurrence. In addition, we found that the anomalies have an extreme value in each of the 5°-23° and 23°-55° and reach a maximum at around 40 degrees with the increase of latitude. Secondly, the anomalies are characterized by large near-summer and small near-winter. In the eddy-center coordinate system, the minus gradient direction of the negative anomaly is consistent with the background flow field and the direction of eddy movement. Meanwhile, the anomaly increases along the radial direction to about 0.2r and then decreases. Finally, there is a significant linear correlation between the anomaly magnitude and eddy amplitude. The conclusion of this research and related mechanism explanation contributes to marine biology research and conservation, estimates of marine primary productivity, and understanding of the biogeochemical properties of eddy modulation in the upper water column.

Plain Language Summary

Euphotic zone is the uppermost body of water in the ocean that receives sunlight. As a rotating water body with a scale of several hundred kilometers, mesoscale eddies affect the depth of the euphotic zone through horizontal and vertical water mass transportation. Using remote sensing data, we analyzed the characteristics of the euphotic zone depth in the mesoscale eddies. The results indicate that anticyclones mainly deepen the euphotic zone depth, while cyclones do the opposite. Eddy-induced euphotic zone depth is inversely correlated with the eddy-induced chlorophyll concentration. Meanwhile, the euphotic zone depth reaches a maximum at around 40 degrees. The conclusions of this research contribute to marine biology research and conservation, estimates of marine primary productivity, and understanding of the biogeochemical properties of eddy modulation in the upper water column.

1 Introduction

The euphotic zone, the foundation of the marine ecosystem, is the uppermost body of water that receives sunlight, enabling phytoplankton to perform photosynthesis. Ninety percent of marine life lives in the euphotic zone, and ninety-five percent of photosynthesis in the ocean occurs in the euphotic zone (Kirk, 1994). As a quantification of the euphotic zone, the bottom depth of the euphotic zone (hereafter referred to as “ZEU”) is a crucial input parameter for many models to estimate basin-scale primary production. (Behrenfeld & Falkowski, 1997a, 1997b). Furthermore, because ZEU reflects the biogeochemical properties of the upper water column, climate-related changes in the marine environment will respond to ZEU (Shang et al., 2011). The hunting time of the olive ridley sea turtle increased with the shallower depth of the euphotic zone and the lower water temperature (Chambault et al., 2016). The light conditions were favorable for the growth of phytoplanktonic when the ratio of ZEU to mixed layer depth was 0.3413 (Khanna et al., 2009).

ZEU is one of the parameters describing the optical properties of seawater. In physics, ZEU is defined as PAR (Photosynthetic Available Radiation) down to the depth of the surface value of

1% (Kirk, 1994). In biology, it is also called compensation depth, which represents the depth at which the net primary productivity (NPP) of phytoplankton equals zero (Behrenfeld & Falkowski, 1997a; Falkowski, 1994). Currently, the calculation of the large area of ZEU mainly comes from remote sensing inversion. One is an empirical algorithm based on CHL concentration (Kratzer et al., 2003; Morel et al., 2007), and the other is a semi-analytical algorithm based on radiative transfer theory that uses the relationship between ZEU and diffuse attenuation coefficient K to calculate (Lee et al., 2007; Mueller & Lange, 2003). ZEU is mainly determined by the water's dissolved, suspended organic matter and inorganic matter concentrations. Usually, ZEU is shallower in offshore water due to terrigenous substances, while ZEU can reach up to180 m in the open ocean (Morel et al., 2007).

Mesoscale eddies are rotating bodies of water that persist for weeks to years and can reach horizontal scales of hundreds of kilometers and penetrate thousands of meters into the ocean interior. These coherent features can modulate primary productivity by changing biophysical-chemical properties such as the nutrition and heat flux of the internal water mass (Danabasoglu et al., 1994; Zhang et al., 2016).

The research results are abundant in the eddy-induced concentration of chlorophyll (CHL), mixed layer, and marine organisms. Half of the chlorophyll in the ocean is trapped by the eddy (Zhao et al., 2021). Studies have shown that anticyclones have higher near-surface CHL than cyclones in subtropical regions (Dufois et al., 2016; Gaube et al., 2013; He et al., 2021), which is contrary to the general characteristics in middle latitudes (Benitez-Nelson et al., 2007; Dawson et al., 2018; Frenger et al., 2018). For Deep Chlorophyll Maxima (DCM), Cyclonic eddies increase the occurrence of DCMs characterized by deep biomass maxima of phytoplankton by providing nutrient conditions and optimal light. Conversely, DCMs in anticyclonic eddies are considered as be driven by photosynthesis. (Cornec et al., 2021). Anticyclones deepen the mixed layer depth, whereas cyclones thin it, and the magnitude of eddy-induced mixed layer depth anomalies is most significant in winter (Gaube et al., 2018). The interaction of wind-driven currents with mesoscale eddies could suppress upwelling in cyclonic eddies and generate upwelling in anticyclonic eddies (Chow et al., 2021; McGillicuddy et al., 2007). Anticyclonic eddies could upwell nutrients below the euphotic zone by generating cyclonic surface stress curl and upward Ekman pumping velocities (Gaube et al., 2013). Pelagic predator catches increased in anticyclonic eddies than cyclones and non-eddy (Arostegui et al., 2022). Research on eddy ecology has developed rapidly in the last decade. However, ZEU characteristics in mesoscale eddies remain unknown. Variations in ZEU are essential for the magnitude of primary and secondary productivity and assessment of the environment for the reproduction and development of photosensitive organisms. This study uses a new matching method to quantify the characteristics of eddy-induced ZEU and analyze the mechanisms involved.

2 Materials and Methods

2.1 ZEU datasets

The daily ZEU datasets from January 1998 to December 2020 with a spatial resolution of 1/4°×1/4° are produced by fusing four satellite water color sensor products (Fanton et al., 2009; Maritorena et al., 2010). The data are calculated by using the empirical algorithm based on CHL concentration. The fused data can improve the spatio-temporal coverage of water color data and reduce the impact of single-sensor data noise.

2.2 Eddy datasets

The daily mesoscale eddy identification and tracking dataset distributed by AVISO was used in this study from January 1998 to December 2020 (Mason et al., 2014; Pegliasco et al., 2022; Pujol et al., 2016; Schlax & Chelton, 2016). The eddy identification method expands from each SLA extreme value (an extremely positive value is AE and an extremely negative value is CE) to form the eddy. The eddy generated by this method has a low computational cost and is easy to extend to three dimensions.

2.3 ZEU data preprocessing

We limit the minimum lifetime of the eddy to 4 weeks to eliminate the effect of transient and eddies resulting from the interpolation procedure.

The ZEU data use a 7-day interpolation time to filter out small-scale ZEU changes caused by a short period and increase the amount of data matching the eddy (Table 1). Only data deeper than 2000 m are used to reduce the disadvantages of the empirical algorithm for coastal water. The bathymetric data were obtained from ETOPO1 Bedrock published by the National Geophysical Data Center (Amante & Eakins, 2009).

ZEU data effective		
sensor	MODIS	Multi-sensor fusion
Raw data	15.61%	28.90%
Processed data	61.23%	74.49%

Table 1. On January 1, 2005, the total number of grids with valid data was divided by the total number deeper than 2000 m above the geoid.

2.4 Effective Eddy matching using the ZEU data

The distance(D) of the grid center from the eddy center was normalized by the eddy radial radius (R). Each eddy was matched with the valid ZEU data on the same date, and the center of the gird coordinates, ZEU value, azimuth angle (θ), and relative radius (r) were recorded within 2.5 r (Figure 1). The eddy effective contour is defined as the largest contour of the detected eddy. Compared with the matching method of fitting contours with a circle, an effective contour is more advantageous for analyzing the eddy 3D structure and submesoscale eddies. Meanwhile, which can preserve the anisotropy of eddy. We divide the eddy from inside to outside into eddy core(0-0.5r), eddy inside(0-1r), eddy disturbance(0-1.5r), and eddy periphery (1.5r-2.5r, the filled area in Figure 1).

$$r = D/R \quad (1)$$

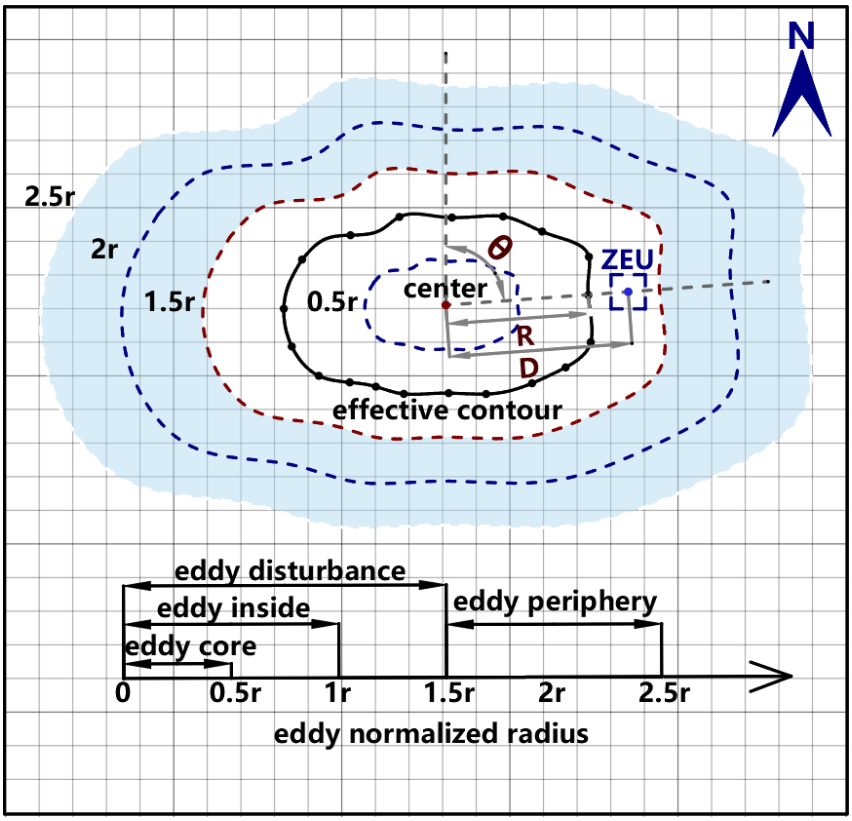

Figure 1. Schematic diagram of normalized radius calculation

2.5 Anomalies of ZEU

Anomalies of the ZEU (ZEU′) at a given location of the grid center (x, y) and time t are defined as

$$ZEU'(x,y,t) = ZEU(x,y,t) - \overline{ZEU}(eddy,t) \quad (2)$$

where $\overline{ZEU}(eddy,t)$ is the mean of ZEU in the eddy periphery. Each eddy has a unique climatological value for each day. The method of calculation not only preserves the seasonal variation about eddy-induced ZEU′ and regional characteristics much as possible but also more accurately calculates the effective eddy-induced ZEU′ by subtracting climatological ZEU with a more significant geographic correlation.

3 Results

3.1 ZEU′ in eddy global distribution

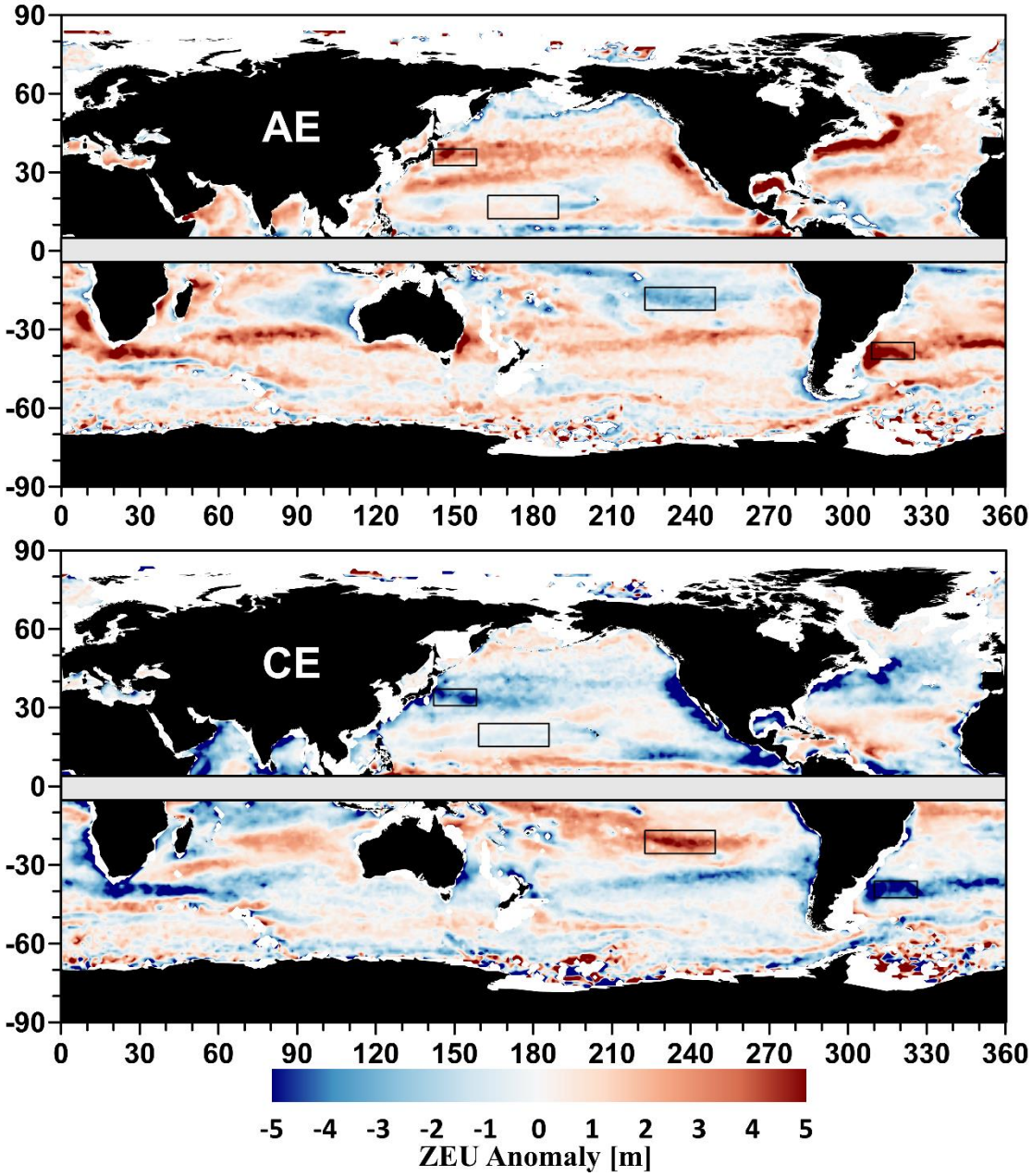

Figure 2. Eddy-induced ZEU′ in eddy inside mapped to a global 1° grid. The regional scopes of the detailed analysis are as follows: Kuroshio Extension (34°N-40°N,144°E-160°E), North Pacific Ocean (15° N-23° N,160° E-172° W), South Pacific Ocean (15° S-23° S,110° W-138° W), and Southwest Atlantic Ocean (34° S-40° S,34° W-50° W).

The selected regions represent areas of boundary currents and are opposite to the general ZEU′ (Figure 2). From the worldwide distribution map of ZEU′ in eddy inside, AE mainly deepens the ZEU, generating positive ZEU′, while CE mainly shoals the ZEU, resulting in negative ZEU′. The ZEU′ caused by eddies with different polarities shows a similar pattern.

However, the ZEU′ of some regions is opposite globally and is mainly distributed in the southern Indian Ocean and the South Pacific. The eddy-induced ZEU varies by more than 5 m in the boundary currents. The ZEU′ in the subtropical gyres are relatively small, with an average range of approximately 1 m.

3.2 Zonal variation of ZEU′

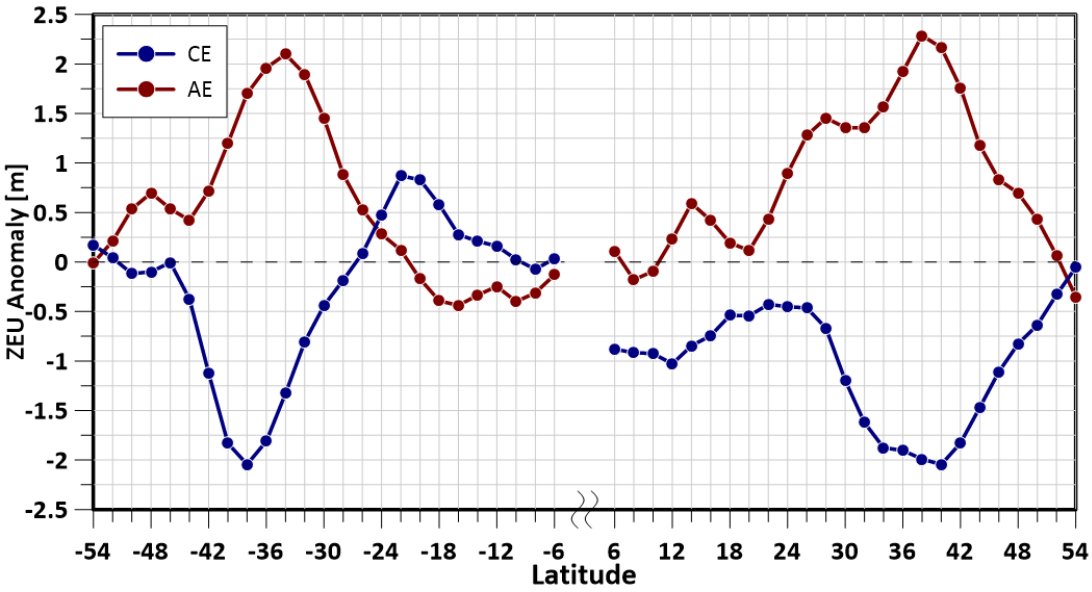

Figure 3. The variation of ZEU′ in the eddy inside with latitude. The ZEU′ of every two degrees was averaged from 5°~ 55°.

The minimum latitudes selected are because the Coriolis force is close to zero, the geostrophic effect fails, and there is almost no mesoscale eddy lasting more than four weeks. In addition, due to the influence of illumination, water color sensor data are insufficient at high latitudes, especially in the Southern Hemisphere winter and the Northern Hemisphere summer. According to the changing curve in Figure 3, to further explore the characteristics of ZEU′, it was divided into four latitudes: the middle latitudes in the Northern Hemisphere (23°N-52°N, NM), the lower latitudes in the Northern Hemisphere (5°N-23°N, NL), the lower latitudes in the Southern Hemisphere (5°S-23°S, SL) and the middle latitudes in the Southern Hemisphere (23°S-52°S, SM).

Globally, ZEU′ induced by AE and CE is symmetrically distributed in the Northern and Southern Hemispheres with latitude. In the lower latitudes, the ZEU′ is small, and in the middle and high latitudes, the ZEU′ is relatively larger. Moreover, AE (CE) induces the positive (negative) ZEU′, which increases first, decreases with latitude, and reaches the maximum at approximately 40°. In the Northern Hemisphere, AE (CE) always induces positive (negative) ZEU′. At lower latitudes, the mean value of AE (CE)-caused ZEU′ was +0.20 m (-0.76 m), and the maximum value was +0.59 m (-1.03 m). In the middle-high latitudes, the mean value of ZEU′ caused by AE (CE) was +1.18 m (-1.15 m), and the maximum value was +2.29 m (-2.05 m). In the Southern Hemisphere, AE (CE) caused negative (positive) ZEU′ at low latitudes with a mean value of -0.26 m (+0.32 m) and a maximum value of -0.44 m (+0.87 m). With the increase of latitude, ZEU′ caused by AE (CE) shift becomes positive (negative) at 22 degrees (26 degrees). Finally, the mean ZEU′ caused by AE (CE) at middle latitudes is +0.94 m (-0.59 m), and the

maximum ZEU′ is +2.10 m (-2.04 m). Compared with the Southern and Northern Hemisphere, the mean value of ZEU′ caused by AE (CE) in the Northern Hemisphere is +0.83 m (-1.01 m), and that in the Southern Hemisphere is +0.51 m (-0.26 m) (Table 2).

	AE	AE means		AE maximum	CE	CE means		CE maximum
NL	-	-0.26	0.51	-0.44	+	0.32	-0.26	+0.87
NM	+	0.94		2.10	-	-0.59		-2.04
SL	+	0.20	0.83	0.59	-	-0.76	-1.01	-1.03
SM	+	1.18		2.29	-	-1.15		-2.05

Table 2. ZEU′ statistics table

3.3 Seasonal variation of ZEU

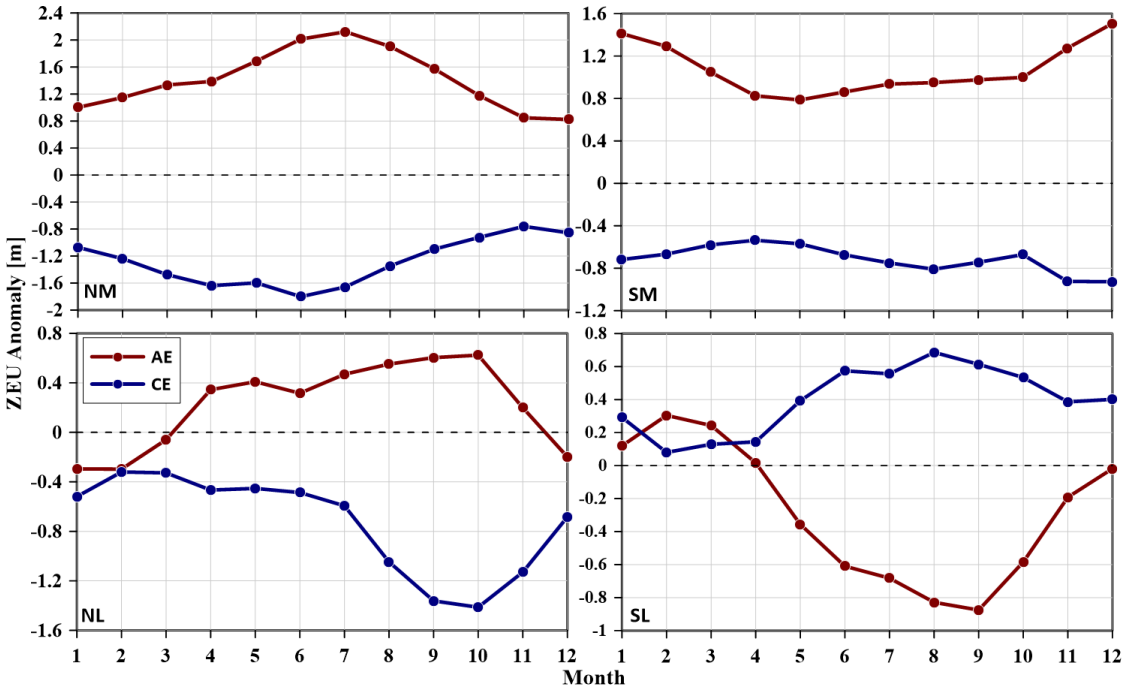

Figure 4. Seasonal variation of ZEU′ in eddy inside.

In the lower latitudes of the Southern (Northern) hemisphere, the ZEU′ in AE is negative (positive) in December-March (January-April), positive (negative) in other months, and reaches the maximum in October (September), which is 0.62 m (-0.88 m) respectively; the ZEU′ in CE is negative (positive) and reached the maximum in October (August), which is -1.41 m (0.69 m) respectively. In the middle latitudes, AE (CE) always causes positive (negative) ZEU′ regardless of the Northern and Southern Hemispheres. ZEU′ is more significant in summer and minor in winter. The maximum ZEU′ induced by AE/CE in the Northern (Southern) hemisphere was +2.1 m/-1.80 m (+1.54 m/-0.90 m).

3.4 Variation of ZEU′ with normalized radius in a two-dimensional eddy coordinate system

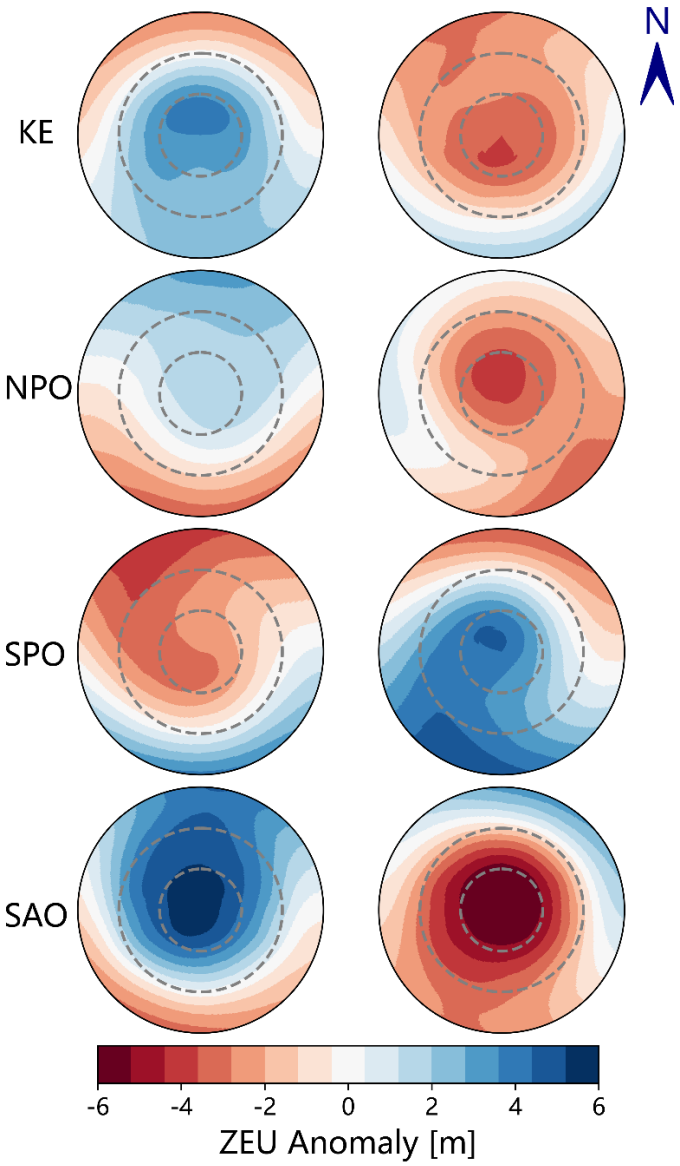

Figure 5. Two-dimensional distributed graph of ZEU′ with normalized radius in eddy disturbance with the left column in AE and the right column in CE. ZEU′ are linearly interpolated into a 150*360 grid and drawn in polar coordinates. From top to bottom, there are four regions: KE, NPO, SPO, and SAO. The inner-dashed circle is 0.5r, the middle-dashed circle is 1r, and the outermost circle is 1.5r.

The ZEU′ caused by the eddy is not a single positive or negative within 1.5r of the eddy, and AE(CE) causes the opposite positive (negative) ZEU′ within 1r except in the South Pacific globally. The ZEU′ in the two regions of the middle latitudes is more prominent than those in the low latitudes. The eddy has a dipole phenomenon in the low-latitude region. The coupling direction is consistent with the rotation direction of different polar eddies in the Northern and

Southern Hemispheres. CE rotates clockwise in the Northern Hemisphere, AE rotates counterclockwise, and the Southern Hemisphere opposite.

3.5 Variation of ZEU′ with normalized radius in eddy coordinate system

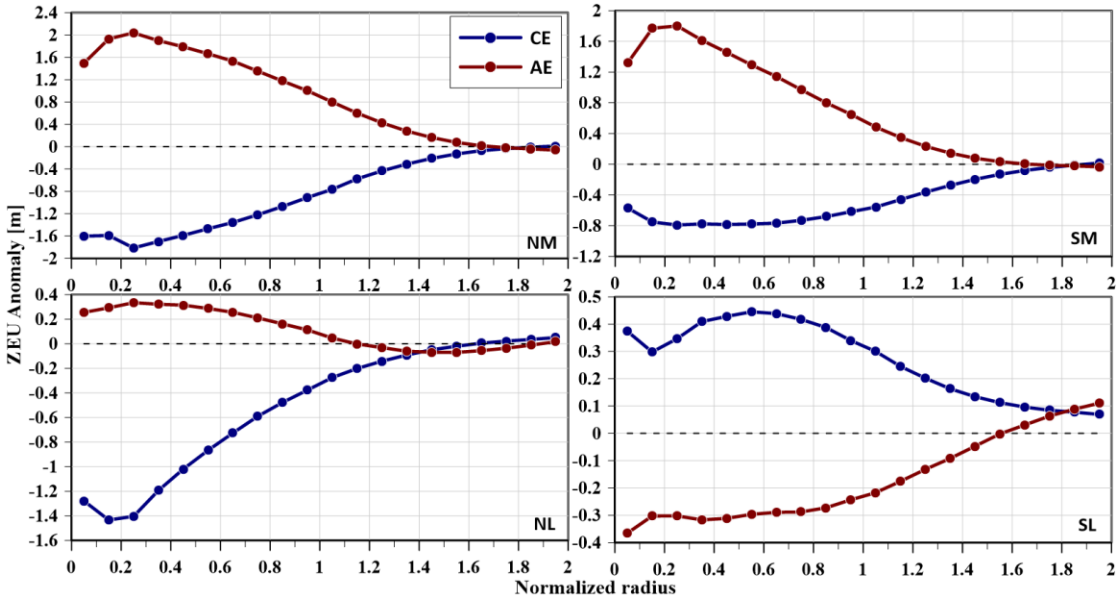

Figure 6. The graph of ZEU′ with normalized radius at different latitudes. The radius interval is 0.1.

ZEU′ intensity decreases along with the relative radius on the whole. In NL, the positive (negative) ZEU′ caused by AE (CE) increases first and then decreases from the center, reaching approximately zero at around 1r (1.5r). In SL, the positive (negative) ZEU′ caused by CE (AE) first decreased, then increased, and then reduced from the center. ZEU′ induced by AE approaches zero near 1.5r and then becomes positive, which in CE is still a negative ZEU′. In the middle latitudes, the intensity of ZEU′ caused by eddies increases first, decreases along the normalized radius from the center, and approaches zero at approximately 1.6r.

	AE maximum	AE	CE maximum	CE
SL	0	~1.5r	~0.5r	>2.0r
SM	~0.2r	~1.6r	~0.2r	~1.8r
NL	~0.2r	1.1r	~0.2r	~1.5r
NM	~0.2r	1.7r	~0.2r	~1.7r

Table 3. Normalized radius position of the ZEU′ maximum and zero point

3.6 ZEU′ quantization in eddy

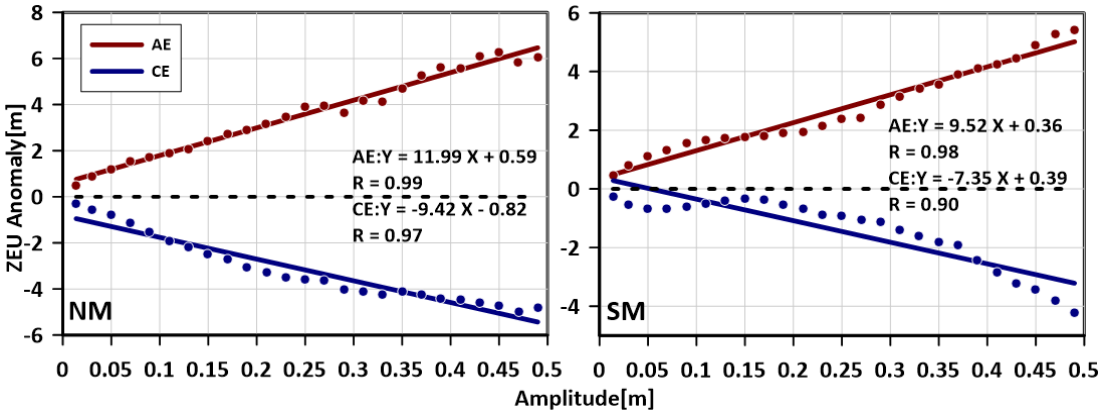

Figure 7. ZEU′ as a function of eddy amplitude. Mean amplitude and ZEU′ were calculated at 2 cm intervals in the eddy core. Solid lines result from a linear fit($p<0.01$).

In the lower latitudes, eddy pumping is not always the dominant mechanism (McGillicuddy, 2016), and the correlation coefficient between anomaly and amplitude is relatively low. Therefore, the relationship between ZEU′ and amplitude in lower latitudes is not shown. In the middle latitudes, the anomaly in the eddy core is relatively significant and only unipolar. The ZEU′ caused by the eddy positively correlates with the eddy amplitude. At the same amplitude, AE had a more significant effect on the ZEU′ than CE. In comparison between the Northern and Southern Hemispheres, the Northern Hemisphere eddy with the same amplitude causes a larger ZEU′ than the Southern Hemisphere eddy. The correlation is also better than other latitudes.

4 Discussion and Conclusions

The ZEU of the global open ocean is mainly negatively correlated with CHL (Morel et al., 2007). The ZEU′ caused by the eddy is consistent with the eddy-induced CHL. Therefore, the geographical distribution of the two anomalies has a consistent pattern and opposite polarity. The intensity of the anomaly is closely related to the eddy-prone area and the distribution of eddy kinetic energy. The primary mechanism of eddy modulation on ZEU is that the upwelling (downwelling) flows caused by CE (AE) increase (decrease) the nutrient supply from the subsurface layer to the surface layer, promote (inhibit) the growth of phytoplankton and increase (decreases) the CHL (Behrenfeld & Falkowski, 1997b; Chelton et al., 2011; McGillicuddy & Robinson, 1997). The exceptional cases, in regions such as the southern Indian Ocean and the South Pacific, may be due to the upwelling (downwelling) flows of CE (AE) that make the mixed layer shallower (deeper) and make fewer (more) nutrients available to phytoplankton in the upper mixed layer, thus reducing (increasing) the concentration of phytoplankton (Dufois et al., 2014). An alternative explanation is that plant photoacclimation caused by deepened mixing, and faster light attenuation leads to higher CHL in AE and the opposite in CE. The phytoplankton changes the cellular pigmented concentration by physiological adjustments in the subtropical gyres (He et al., 2021). In nutrient-limited conditions, eddy-induced Ekman pumping would yield positive CHL anomaly in AE and negative CHL anomaly in CE (Dewar & Flierl, 1987; Travis & Qiu, 2020). Multiple mechanisms have generated the observed global ZEU′ pattern based on the above.

When the two polar eddies act on the euphotic zone, the latitudinal variation of ZEU′ is related to the variation of the latitudinal amplitude of the eddy. The anomaly is minor in lower latitudes, more significant in middle latitudes, and reaches a maximum of approximately 40 degrees. Regardless of AE and CE, the average effect on ZEU in the Northern Hemisphere is more significant than in the Southern Hemisphere.

The ZEU′ caused by the eddy has prominent seasonal characteristics. In the lower latitudes, the anomalies are larger in near-summer in the Northern Hemisphere and larger in near-winter in the Southern Hemisphere. In the middle latitudes, the ZEU′ caused by eddies is the largest in summer and the smallest in winter. A change in ZEU′ polarity will occur in March and April in lower latitudes. The upwelling/downwelling flow pumping caused by CE/AE was the primary mechanism in the Northern Hemisphere. With the stronger stratification from July to November, the nutrient supply from the subsurface layer to the near-surface layer was inhibited, while eddy pumping on chlorophyll was relatively dominant. In the Southern Hemisphere, the eddy kinetic energy is weak, eddy pumping is no longer the dominant mechanism, and the mixed layer, eddy-wind interaction, and photoacclimation play a dominant role. When the background mixed layer deepens from May to November, the mixed layer anomaly caused by eddies is the largest (Gaube et al., 2019), resulting in the strongest ZEU′.

The ZEU′ is not the strongest in the eddy center and has an extremum at approximately 0.2r, which influence range is 1.6r in middle latitudes and ranges from 1r-2r in lower latitudes. In the eddy coordinate system, the vertical velocity of water masses caused by the eddy pump, eddy-wind interaction, and other dynamic processes decreases from the center to the outside, so the eddy-induced anomalies are consistent with the variation. However, in SL, the opposite ZEU′ caused by other mechanisms is partially counterbalanced until approximately 0.2r. The influence of eddies on the euphotic zone is not limited to 1r but extends to approximately 1.6r in the middle latitudes. In the lower latitudes, the range of eddy perturbations is extended due to the relatively enhanced stirring and trapping mechanism and the submesoscale processes in the eddy peripheries (Gaube et al., 2014; Guo et al., 2019). The eddy has a dipole phenomenon at lower latitudes, and the coupling direction is consistent with the rotation direction of different polar eddies in the Northern and Southern Hemispheres. ZEU′ is more concentrated in the middle latitudes and not easily disturbed by the Coriolis force. Nevertheless, the negative gradient direction of the negative anomaly is consistent with the background flow field and the direction of eddy movement.

There is a significant linear relationship between the eddy amplitude and ZEU′. The eddy with the same amplitude has a more excellent correlation and a more considerable magnitude in the NM. Eddy amplitude positively correlates with eddy kinetic energy (Chelton et al., 2007). The consistency between the ZEU anomaly geographic distribution and eddy kinetic energy intensity distribution indicates that the ZEU anomaly and eddy amplitude are correlated. The Southern Hemisphere is more nutrient deficient than the Northern Hemisphere. The vertical material transport of eddies with the same amplitude will be more significant in the Northern Hemisphere, resulting in a greater ZEU′.

Acknowledgments

This research was jointly supported by the National Natural Science Foundation of China (Grant No.42030406), the Marine S & T Fund of Shandong Province for Pilot National

Laboratory for Marine Science and Technology (No.2022QNLM050301-1), International Research Center of Big Data for Sustainable Development Goals (CBAS2022GSPO1) and Ocean University of China (GrantNo.202251004).

Data Availability Statement

GlobColour data (http://globcolour.info) used in this study has been developed, validated, and distributed by ACRI-ST, France.

The Altimetric Mesoscale Eddy Trajectories Atlas (META3.2 DT) was produced by SSALTO/DUACS and distributed by AVISO+ (https://aviso.altimetry.fr) with support from CNES in collaboration with IMEDEA (DOI: 10.24400/527896/a01-2022.005.220209 for the META3.2 DT allsat version).

ETOPO1 Global Relief Model is used to calculate sea depth above the geoid (https://www.ngdc.noaa.gov/mgg/global/global.html) (DOI: 10.7289/V5C8276M).

References

Amante, C., & Eakins, B. W. (2009). ETOPO1 1 Arc-Minute Global Relief Model: Procedures, Data Sources and Analysis. In *NOAA Technical Memorandum NESDIS NGDC-24*. National Geophysical Data.

Arostegui, M. C., Gaube, P., Woodworth-Jefcoats, P. A., Kobayashi, D. R., & Braun, C. D. (2022, Sep). Anticyclonic eddies aggregate pelagic predators in a subtropical gyre. *Nature, 609*(7927), 535-540. https://doi.org/10.1038/s41586-022-05162-6

Behrenfeld, M. J., & Falkowski, P. G. (1997a, Nov). A consumer's guide to phytoplankton primary productivity models. *Limnology and Oceanography, 42*(7), 1479-1491. https://doi.org/DOI 10.4319/lo.1997.42.7.1479

Behrenfeld, M. J., & Falkowski, P. G. (1997b, Jan). Photosynthetic rates derived from satellite-based chlorophyll concentration. *Limnology and Oceanography, 42*(1), 1-20. https://doi.org/DOI 10.4319/lo.1997.42.1.0001

Benitez-Nelson, C. R., Bidigare, R. R., Dickey, T. D., Landry, M. R., Leonard, C. L., Brown, S. L., Nencioli, F., Rii, Y. M., Maiti, K., Becker, J. W., Bibby, T. S., Black, W., Cai, W. J., Carlson, C. A., Chen, F., Kuwahara, V. S., Mahaffey, C., McAndrew, P. M., Quay, P. D., Rappe, M. S., Selph, K. E., Simmons, M. P., & Yang, E. J. (2007, May 18). Mesoscale eddies drive increased silica export in the subtropical Pacific Ocean. *Science, 316*(5827), 1017-1021. https://doi.org/10.1126/science.1136221

Chambault, P., de Thoisy, B., Heerah, K., Conchon, A., Barrioz, S., Dos Reis, V., Berzins, R., Kelle, L., Picard, B., Roquet, F., Le Maho, Y., & Chevallier, D. (2016, Mar). The influence of oceanographic features on the foraging behavior of the olive ridley sea turtle Lepidochelys olivacea along the Guiana coast. *Progress in Oceanography, 142*, 58-71. https://doi.org/10.1016/j.pocean.2016.01.006

Chelton, D. B., Gaube, P., Schlax, M. G., Early, J. J., & Samelson, R. M. (2011, Oct 21). The influence of nonlinear mesoscale eddies on near-surface oceanic chlorophyll. *Science, 334*(6054), 328-332. https://doi.org/10.1126/science.1208897

Chelton, D. B., Schlax, M. G., Samelson, R. M., & de Szoeke, R. A. (2007, Aug 9). Global observations of large oceanic eddies. *Geophysical Research Letters, 34*(15). https://doi.org/Artn L15606 10.1029/2007gl030812

Chow, C. H., Shih, Y. Y., Chien, Y. T., Chen, J. Y., Fan, N., Wu, W. C., & Hung, C. C. (2021, Aug 19). The Wind Effect on Biogeochemistry in Eddy Cores in the Northern South China Sea. *Frontiers in Marine Science, 8*. https://doi.org/ARTN 717576 10.3389/fmars.2021.717576

Cornec, M., Laxenaire, R., Speich, S., & Claustre, H. (2021, Aug 16). Impact of Mesoscale Eddies on Deep Chlorophyll Maxima. *Geophys Res Lett*, *48*(15), e2021GL093470. https://doi.org/10.1029/2021GL093470

Danabasoglu, G., McWilliams, J. C., & Gent, P. R. (1994, May 20). The role of mesoscale tracer transports in the global ocean circulation. *Science*, *264*(5162), 1123-1126. https://doi.org/10.1126/science.264.5162.1123

Dawson, H. R. S., Strutton, P. G., & Gaube, P. (2018, Sep). The Unusual Surface Chlorophyll Signatures of Southern Ocean Eddies. *Journal of Geophysical Research-Oceans*, *123*(9), 6053-6069. https://doi.org/10.1029/2017jc013628

Dewar, W. K., & Flierl, G. R. (1987). Some Effects of the Wind on Rings. *Journal of physical oceanography*, *17*(10), 1653-1667. https://doi.org/10.1175/1520-0485(1987)017<1653:Seotwo>2.0.Co;2

Dufois, F., Hardman-Mountford, N. J., Greenwood, J., Richardson, A. J., Feng, M., Herbette, S., & Matear, R. (2014, Nov). Impact of eddies on surface chlorophyll in the South Indian Ocean. *Journal of Geophysical Research-Oceans*, *119*(11), 8061-8077. https://doi.org/10.1002/2014jc010164

Dufois, F., Hardman-Mountford, N. J., Greenwood, J., Richardson, A. J., Feng, M., & Matear, R. J. (2016, May). Anticyclonic eddies are more productive than cyclonic eddies in subtropical gyres because of winter mixing. *Sci Adv*, *2*(5), e1600282. https://doi.org/10.1126/sciadv.1600282

Falkowski, P. G. (1994, Mar). The role of phytoplankton photosynthesis in global biogeochemical cycles. *Photosynth Res*, *39*(3), 235-258. https://doi.org/10.1007/BF00014586

Fanton , O., Mangin, A., Lavender, S., Antoine, D., Maritorena, S., Morel, A., Barrot, G., Demaria, J., & Pinnock, S. (2009). GlobColour-the European Service for Ocean Colour. Proceedings from 2009 IEEE International Geoscience & Remote Sensing Symposium (IGARSS),

Frenger, I., Munnich, M., & Gruber, N. (2018, Aug 13). Imprint of Southern Ocean mesoscale eddies on chlorophyll. *Biogeosciences*, *15*(15), 4781-4798. https://doi.org/10.5194/bg-15-4781-2018

Gaube, P., Braun, C. D., Lawson, G. L., McGillicuddy, D. J., Jr., Penna, A. D., Skomal, G. B., Fischer, C., & Thorrold, S. R. (2018, May 9). Mesoscale eddies influence the movements of mature female white sharks in the Gulf Stream and Sargasso Sea. *Sci Rep*, *8*(1), 7363. https://doi.org/10.1038/s41598-018-25565-8

Gaube, P., Chelton, D. B., Strutton, P. G., & Behrenfeld, M. J. (2013, Dec). Satellite observations of chlorophyll, phytoplankton biomass, and Ekman pumping in nonlinear

mesoscale eddies. *Journal of Geophysical Research-Oceans, 118*(12), 6349-6370. https://doi.org/10.1002/2013jc009027

Gaube, P., McGillicuddy, D. J., Chelton, D. B., Behrenfeld, M. J., & Strutton, P. G. (2014, Dec). Regional variations in the influence of mesoscale eddies on near-surface chlorophyll. *Journal of Geophysical Research-Oceans, 119*(12), 8195-8220. https://doi.org/10.1002/2014jc010111

Gaube, P., McGillicuddy, D. J., & Moulin, A. J. (2019, Feb 16). Mesoscale Eddies Modulate Mixed Layer Depth Globally. *Geophysical Research Letters, 46*(3), 1505-1512. https://doi.org/10.1029/2018gl080006

Guo, M. X., Xiu, P., Chai, F., & Xue, H. J. (2019, Nov 28). Mesoscale and Submesoscale Contributions to High Sea Surface Chlorophyll in Subtropical Gyres. *Geophysical Research Letters, 46*(22), 13217-13226. https://doi.org/10.1029/2019gl085278

He, Q. Y., Zhan, H. G., Cai, S. Q., & Zhan, W. K. (2021, Apr 16). Eddy-Induced Near-Surface Chlorophyll Anomalies in the Subtropical Gyres: Biomass or Physiology? *Geophysical Research Letters, 48*(7). https://doi.org/ARTN e2020GL091975 10.1029/2020GL091975

Khanna, D. R., Bhutiani, R., & Chandra, K. S. (2009, Spr). Effect of the Euphotic Depth and Mixing Depth on Phytoplanktonic Growth Mechanism. *International Journal of Environmental Research, 3*(2), 223-228. <Go to ISI>://WOS:000264304700007

Kirk, J. T. O. (1994). *Light and photosynthesis in aquatic ecosystems* (2019/10/09 ed., Vol. 74). Cambridge University Press. https://doi.org/10.1017/S0025315400090366

Kratzer, S., Hakansson, B., & Sahlin, C. (2003, Dec). Assessing Secchi and photic zone depth in the Baltic Sea from satellite data. *Ambio, 32*(8), 577-585. https://doi.org/10.1579/0044-7447-32.8.577

Lee, Z., Weidemann, A., Kindle, J., Arnone, R., Carder, K. L., & Davis, C. (2007, Mar 16). Euphotic zone depth: Its derivation and implication to ocean-color remote sensing. *Journal of Geophysical Research-Oceans, 112*(C3). https://doi.org/Artn C03009 10.1029/2006jc003802

Maritorena, S., d'Andon, O. H. F., Mangin, A., & Siegel, D. A. (2010, Aug 16). Merged satellite ocean color data products using a bio-optical model: Characteristics, benefits and issues. *Remote Sensing of Environment, 114*(8), 1791-1804. https://doi.org/10.1016/j.rse.2010.04.002

Mason, E., Pascual, A., & McWilliams, J. C. (2014, May). A New Sea Surface Height-Based Code for Oceanic Mesoscale Eddy Tracking. *Journal of Atmospheric and Oceanic Technology, 31*(5), 1181-1188. https://doi.org/10.1175/Jtech-D-14-00019.1

McGillicuddy, D. J., Jr. (2016). Mechanisms of Physical-Biological-Biogeochemical Interaction at the Oceanic Mesoscale. *Ann Rev Mar Sci, 8*, 125-159. https://doi.org/10.1146/annurev-marine-010814-015606

McGillicuddy, D. J., Jr., Anderson, L. A., Bates, N. R., Bibby, T., Buesseler, K. O., Carlson, C. A., Davis, C. S., Ewart, C., Falkowski, P. G., Goldthwait, S. A., Hansell, D. A., Jenkins, W. J., Johnson, R., Kosnyrev, V. K., Ledwell, J. R., Li, Q. P., Siegel, D. A., & Steinberg, D. K. (2007, May 18). Eddy/wind interactions stimulate extraordinary mid-ocean plankton blooms. *Science, 316*(5827), 1021-1026. https://doi.org/10.1126/science.1136256

McGillicuddy, D. J., & Robinson, A. R. (1997, Aug). Eddy-induced nutrient supply and new production in the Sargasso Sea. *Deep-Sea Research Part I-Oceanographic Research Papers, 44*(8), 1427-1450. https://doi.org/Doi 10.1016/S0967-0637(97)00024-1

Morel, A., Huot, Y., Gentili, B., Werdell, P. J., Hooker, S. B., & Franz, B. A. (2007, Nov 15). Examining the consistency of products derived from various ocean color sensors in open ocean (Case 1) waters in the perspective of a multi-sensor approach. *Remote Sensing of Environment, 111*(1), 69-88. https://doi.org/10.1016/j.rse.2007.03.012

Mueller, J. L., & Lange, R. E. (2003). Bio‐optical provinces of the Northeast Pacific Ocean: A provisional analysis. *Limnology and Oceanography, 34*(8), 1572-1586. https://doi.org/10.4319/lo.1989.34.8.1572

Pegliasco, C., Delepoulle, A., Mason, E., Morrow, R., Faugere, Y., & Dibarboure, G. (2022, Mar 10). META3.1exp: a new global mesoscale eddy trajectory atlas derived from altimetry. *Earth System Science Data, 14*(3), 1087-1107. https://doi.org/10.5194/essd-14-1087-2022

Pujol, M. I., Faugere, Y., Taburet, G., Dupuy, S., Pelloquin, C., Ablain, M., & Picot, N. (2016, Sep 9). DUACS DT2014: the new multi-mission altimeter data set reprocessed over 20 years. *Ocean Science, 12*(5), 1067-1090. https://doi.org/10.5194/os-12-1067-2016

Schlax, M. G., & Chelton, D. B. (2016). The "growing method" of eddy identification and tracking in two and three dimensions. *College of Earth, Ocean and Atmospheric Sciences, Oregon State University, Corvallis, Oregon, 8*.

Shang, S. L., Lee, Z. P., & Wei, G. M. (2011, Jan 17). Characterization of MODIS-derived euphotic zone depth: Results for the China Sea. *Remote Sensing of Environment, 115*(1), 180-186. https://doi.org/10.1016/j.rse.2010.08.016

Travis, S., & Qiu, B. (2020, Mar). Seasonal Reversal of the Near-Surface Chlorophyll Response to the Presence of Mesoscale Eddies in the South Pacific Subtropical Countercurrent. *Journal of Geophysical Research-Oceans, 125*(3). https://doi.org/ARTN e2019JC015752 10.1029/2019JC015752

Zhang, Z., Tian, J., Qiu, B., Zhao, W., Chang, P., Wu, D., & Wan, X. (2016, Apr 14). Observed 3D Structure, Generation, and Dissipation of Oceanic Mesoscale Eddies in the South China Sea. *Sci Rep, 6*, 24349. https://doi.org/10.1038/srep24349

Zhao, D. D., Xu, Y. S., Zhang, X. G., & Huang, C. (2021, Mar 1). Global chlorophyll distribution induced by mesoscale eddies. *Remote Sensing of Environment, 254*. https://doi.org/ARTN 112245
10.1016/j.rse.2020.112245